Acoustic Mine Detection Using the Navy's CASS/GRAB Model

Peter C. Chu, Carlos Cintron, Steven D. Haeger, Ruth E. Keenan

***Abstract*-- The purpose of this work is to determine the necessity of a near real time ocean modeling capability such as the Naval Oceanographic Office's (NAVOCEANO) Modular Ocean Data Assimilation System (MODAS) model in shallow water (such as the Yellow Sea) mine hunting applications using the Navy's Comprehensive Acoustic Simulation System/Gaussian Ray Bundle (CASS/GRAB) model. Sound speed profiles inputted into the CASS/GRAB were calculated from observational and climatological data sets for different seasons and regions of four different bottom types (sand, gravel, mud, and rock). The CASS/GRAB model outputs were compared to the outputs from corresponding MODAS data sets. The results of the comparisons demonstrated in many cases a significant acoustic difference between the alternate profiles. These results demonstrated that there is a need for a predictive modeling capability such as MODAS to address the Mine Warfare (MIW) needs in the Yellow Sea region. There were some weaknesses detected in the profiles the MODAS model produces in the Yellow Sea, which must be resolved before it can reliably address the MIW needs in that region.**

***Index Terms*—Acoustic mine hunting, Navy's comprehensive acoustic simulation system/Gaussian ray bundle (CASS/GRAB) model, modular ocean data assimilation system (MODAS), master oceanographic observational data set (MOODS), generalized digital environmental model (GDEM).**

INTRODUCTION

The major threats in the littoral are diesel submarines and sea mines. The combination of improvements in noise reducing technology and the development of Air Independent Propulsion (AIP) technology have made diesel submarines very difficult to detect in both the littoral and blue waters. After a weapon platform has detected its targets, the sensors on torpedoes designed for blue water operations are not designed to acquire a target in a reverberation-crippling environment.

Even though sea mines are not as sophisticated a weapons system as torpedoes, they have been number one cause of U.S. Naval casualties since the end of World War II. Sea mines are a relatively cheap weapons system that can be easily obtained by any nation in mass quantities. In addition, Sea mines do not require an expensive and sophisticated weapons platform for deployment; they can be easily deployed by small watercraft. There are several types of mines, which are classified by their mode of activation and their placement in the water column. The simplest of sea mines are floating contact mines. These mines are usually detected visually and cleared by minesweepers and Explosive Ordnance Disposal (EOD) units.

A more complex type of mines is influence mine. These mines have different mechanisms for activation, such as magnetic and acoustic actuators. Influence mines are much more difficult to counter since they are either tethered to the sea bottom at various depths or lie on the sea bottom. Since these types of mines are situated below the sea surface, mine hunting sonars are required for detection. The problems that are related to sonar detection of a target in the littoral are compounded when the target is a sea mine due to the low target strengths of Sea mines. The low target strengths of sea mines require the use of sensors with frequencies higher than those sonars used for submarine detection. Bottom mines create a much more difficult detection problem for the mine hunter. Operators of mine hunting systems must perform the timely process of classifying all objects that closely fit the dimensions of a Bottom mine and later evaluate these objects in closer detail with higher resolution sensors.

In recent years, the U.S. Navy has focused much of its research and development efforts in designing high frequency sensors and corresponding acoustic models to overcome the threat in the littoral. The Comprehensive Acoustic Simulation System (CASS) using the Gaussian Ray Bundle (GRAB) model is an acoustic model approved by the U.S. Navy to predict the performance of active ocean acoustic systems that operate in the 600 Hz to 100 kHz frequency range. Developed in 1993 by the Naval Undersea Warfare Center Division Newport, this model is

Manuscript received January 15, 2002. This work was supported by the U.S. Office of Naval Research, Naval Oceanographic Office, and Naval Postgraduate School.

Peter C. Chu is with the Naval Postgraduate School, Monterey, CA 93943 USA (telephone: 831-677-3688, e-mail: chu@ nps.navy.mil).

C. J. Cintron., is with Naval Postgraduate School, Monterey, CA 93943 USA (e-mail: cjcintro@pacbell.net).

S.D. Haeger is with the Naval Oceanographic Office, Stennis Space Center,MS 39529 USA (e-mail: Haegers@navo.navy.mil).

R.E. Keenan is with the Scientific Application International Corporation, Mashpee, MA 02649 (email: rkeenan@capecod.net).

capable of modeling all the components of passive and bistatic signal excess in range-dependent environments. The CASS/GRAB has successfully modeled torpedo acoustic performance in shallow water experiments off the coast of Southern California and Cape Cod, and is currently being developed to simulate mine warfare systems performance in the fleet (Aidala et al. 1998).

The CASS/GRAB model is valuable tool for the AN/SQQ-32 mine hunting detection and classification sonar. The performance of this model, as in all models, is determined by the accuracy of its inputs such as sea surface conditions, bathymetry, bottom type, and sound speed profiles.

The AN/SQQ-32 is a variable depth mine hunting detection and classification sonar for the Avenger (MCM-1) and Osprey (MHC-51) Surface Mine Countermeasures (SMCM) ships. The AN/SQQ-32's main components are a multi-channel detection sonar assembly and near-photographic resolution classification sonar assembly. The system has multiple operating frequencies and obtains acoustic data from two independent acoustic search and classification arrays that maximize volumetric coverage. Its multiple-ping processor enables it to detect mine-like objects in the high reverberation environment of the littoral. Additionally, its multiple operating frequency capability allows it to operate in both deep and shallow waters. The lower operating frequencies allow the system to detect mine-like objects at longer ranges in shallow waters. The classification sonar system's near-photograph resolution and the systems computer aided target classification system decreases the time required for mine searching operations by reducing false target reporting.

I. ENVIRONMENT OF THE YELOWW SEA

A. Geology and Structure

The Yellow Sea is a semi-enclosed basin situated between China and the Korean peninsula with the Bohai Sea to the northwest and the East China Sea to the south. The Yellow Sea is a large shallow water basin covering an area of approximately 295,000 km^2. The water depth over most of the area is less than 50 m (Fig. 1). Four major fresh water run-offs flow into the Yellow Sea: the Yangtze River to the southwest, the Yellow River and Liao River to the north, and the Han River to the east (Chu et al. 1997a).

Due to large tidal ranges and heavy sedimentation from river outflows, most of the coasts surrounding the Yellow Sea contain numerous shoals and troughs extending from the shores. The bottom sediment types are finer along the coast of China and much coarser along the shelf and the coast of the Korean peninsula. The bottom sediment of the central and western regions of the Yellow Sea consists primarily of mud and the eastern region is primarily sand. The mud sedimentation in the central and northwestern regions of the Yellow Sea is due to the runoff from the great rivers of China (Shepard 1973).

Four regions with different bottom types were selected for the acoustic model runs in this study (Fig. 2). The first region consists of a Rock Bottom type and is located in the north-central Yellow Sea at 37^o-37.5^o N, 123^o-123.8^o E. The second region consists of a Gravel Bottom type and is located in the northern Yellow Sea at 38.4^o-39^o N, 122^o-123^o E. The third region consists of a Sand Bottom type and is located in the southeastern Yellow Sea at 35.5^o-36.5^o N, 124.5^o-126.2^o E. The fourth region consists of a Mud Bottom type and is located in the south-central Yellow Sea at 35^o-36.5^o N, 123^o- 124.5^o E.

B. Oceanography

The four seasons in the Yellow Sea are defined as follows: the winter months run from January through March; the spring months run from April through June; the summer months run from July through September; and the fall months run from October through December.

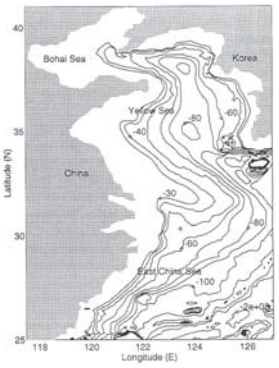

Fig. 1. Bottom Topography of the Yellow Sea and the surrounding regions. (From Chu et al. 1997a).

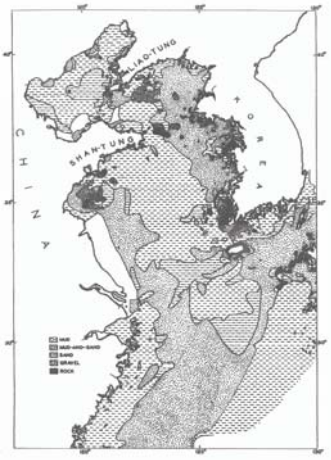

Fig. 2. Yellow Sea Bottom sediment chart (From Ninno and Emery 1961).

The Siberian high-pressure system during the winter monsoon season brings very cold northwest winds through the Yellow Sea region. During this period, the jet stream is located south of the Yellow Sea and the polar front is located north of the Philippines. At the beginning of the winter season the mean wind speed is 6 m/s and the sea air

temperature (SAT) falls in the range of 0^o to 8^o C, where the sea surface temperature (SST) is usually 2^o to 6^o C warmer causing the Yellow Sea to lose heat to the atmosphere during this time period. The winter monsoon winds peak with a maximum of 35 m/s in the central Yellow Sea, and 28 m/s mean through out the entire region (Chu et al. 1997a). These cold/strong winter monsoon winds cause mechanical forcing due to the strong wind stress and thermal forcing resulting from the upward buoyancy flux at the air-ocean interface caused by the cold SAT. The combined action of the mechanical and thermal forcing causes the mixed layer to drop to its deepest point during the winter season.

The transition into the spring season begins in late March. By the end of the first month of spring, the atmospheric polar front has transited northward into Korea followed by warm and humid air masses into the Yellow Sea region. This transition brings about an average increase in the SST of 10^o C during the spring.

The transition into the summer season begins in late May and early June. The movement of this low-pressure system sets up circulation of the southwest monsoon in the Yellow Sea during the summer months. During this period, the jet stream is located south of Korea and the polar front is located south of the Japanese Islands of Kyushu and Shikoku. In July, the atmospheric low-pressure system in the north, in conjunction with an atmospheric high-pressure system located in the southeast called the Bonin High, generates warm and humid southerly winds over the Yellow Sea region. The warm air from these southerly winds increases the SAT over the Yellow Sea during the summer months to a range of 24^o to 26^o C, approximately 1.5^o to 2^o C warmer than the SST. Although there is a high weather activity in the Yellow Sea during the summer monsoon season, the mean wind speed throughout the region only ranges from 3 to 4 m/s. During the summer months, there is also a stronger downward net radiation and this effect, combined with the warmer air, causes a downward heat flux that reduces the depth of the mixed layer (Chu et al. 1997a, b). The summer season is also usually characterized by Tropical Cyclones that transit through the region, moving in a northwest direction from the East China Sea into the southern Yellow Sea and into China. Occasionally, a tropical cyclone will transit in a northerly direction from the East China Sea and throughout the Yellow Sea.

October marks the beginning of the fall season in the Yellow Sea. In October, the warm southerly winds of the summer monsoon begin to subside in the region and the SAT and SST begin to gradually transition to those of the winter season.

The two main characteristic temperature profiles of the Yellow Sea are during the winter and the summer months. In the winter months, the temperature profiles throughout the region are characterized as isothermal (Fig. 3a). In the summer months, the temperature profiles throughout the region are characterized by a multi-layer profile consisting of a mixed layer, a thermocline, and a deep layer (Fig. 3b).

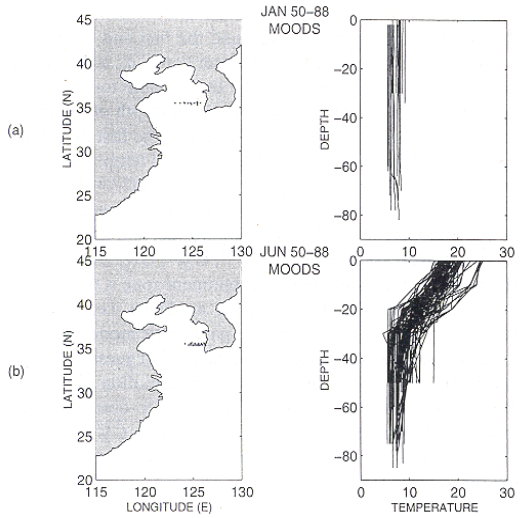

Fig. 3. Eastern Yellow Sea (around 36 N) temperature profiles during 1950-1988; (a) January and (b) June. Solid dots show the location of the observation stations (From Chu et al. 1997b).

2. COMPREHENSIVE ACOUSTIC SIMULATION SYSTEM/ GAUSSIAN RAY BUNDLE (CASS/GRAB)

A. Model Description

CASS/GRAB is an active and passive range dependent propagation, reverberation, and signal excess acoustic model that has been accepted as the Navy's standard model. The GRAB model's main function is to calculate eigenrays in range-dependent environments in the frequency band 600 Hz to 100 kHz and to use the eigenrays to calculate propagation loss. The CASS model is the range dependent improvement of the Generic Sonar model (GSM). CASS performs range independent monostatic and bistatic active signal excess calculations. The CASS model incorporates the GRAB eigenray model as a subset (Fig. 4). CASS uses a driver that calls the GRAB eigenray model to compute eigenrays and propagation loss (Keenan 1998).

In the GRAB model, the travel time, source angle, target angle, and phase of the ray bundles are equal to those values for the classic ray path. The main difference between the GRAB model and a classic ray path is that the amplitude of the Gaussian ray bundles is global, affecting all depths to some degree, whereas classic ray path amplitudes are local. GRAB calculates amplitude globally by distributing the amplitudes according to the Gaussian equation

$$\Psi_\nu = \frac{\beta_{\nu,0}\Gamma_\nu^{\,2}}{\sqrt{2\pi}\,\sigma_\nu\, p_{r,\nu} r} \exp\left\{-0.5\left[(z-z_\nu)/\sigma_\nu\right]^2\right\},$$

where the Γ_ν represents losses due to volume attenuation and boundary interaction, $\sigma_\nu = (0.5)(\max(\Delta z, 4\pi\lambda))$ defines the effective standard deviation of the Gaussian width, and $\beta_{\nu,0}$ is a factor that depends only on the source and is

chosen so that the energy within a geometric-acoustic ray tube equals the energy within a Gaussian ray bundle. The variable z_v is the depth along the v^{th} test ray at range r, z is the target depth, p_r is the horizontal slowness, Δz is the change in ray depth at constant range due to a change in source angle, and λ is the wavelength. The selection of the effective standard deviation σ_v is the weakest component in providing a firm theoretical basis for the GRAB model. The closer the test ray is to the target, the larger the contribution it has to the final power weighted eigenray. These test rays are called ray bundles since they distribute some energy to each depth. GRAB classifies each ray group into a ray family. GRAB version 1.0 defines a ray family as ray groups that have a similar number of surface and bottom bounces. Under caustic conditions there will be ray bundles with surface and bottom depth differences greater than and less than zero within each ray family and GRAB computes an eigenray for each group. Thus, GRAB computes up to two weighted averaged ray groups for each ray family. GRAB does not store all the eigenrays it calculates; instead, it performs a user accessible eigenray tolerance test to determine if eigenrays are too weak to be stored in the eigenray file. GRAB then computes the random or coherent propagation loss from the eigenrays stored in the eigenray file and stores in them in separate pressure files (Aidala et al. 1998).

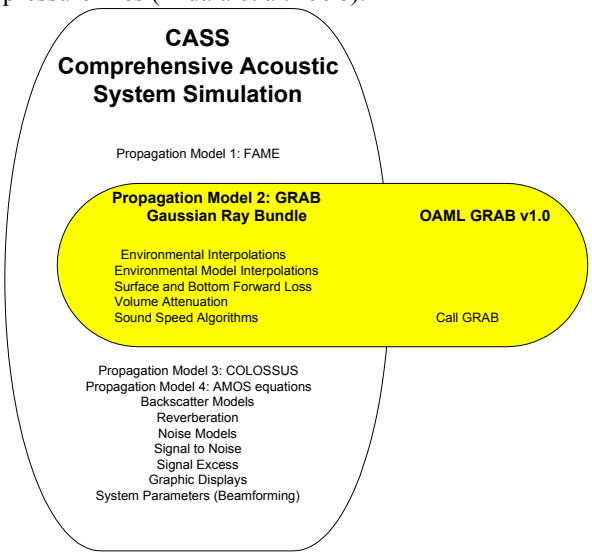

Fig. 4. CASS/GRAB Overview (From Keenan et al. 1999).

CASS computes range dependent reverberation for monostatic and bistatic transmitter to target and target to receiver scenarios. Reverberation is calculated in the time domain centered at the receiver. It accounts for all possible combinations of signal eigenray paths, sums them all up at a given range, and selects the peak signal to noise/ reverberation level to determine signal excess (Keenan 1998).

B. Mine Warfare Scenarios

The high environmental variability and strong multi-path interactions encountered in the littoral make acoustic modeling very difficult. In these shallow water regions, accurate arrival structure information is required to model performance of high frequency acoustic systems. Other Navy range-dependent acoustic models such as the Navy's PE (Parabolic Equation) model are inadequate because they become computationally intensive above several kilohertz. The GRAB eigenray model produces the required arrival structure needed for systems applications in the littoral zone. This capability makes the CASS/GRAB a very effective tool for modeling the performance high frequency acoustic systems in the littoral. In addition, the CASS/GRAB model has successfully modeled torpedo reverberation data in 1994 in shallow water, range dependent environments at the NUWC Southern California (SOCAL) and Cape Cod torpedo exercise areas.

3. SEASONAL VARIABILITY OF ACOUSTIC TRANSMISSION

A. Seasonal Variability of Sound Speed Profiles

The annual mean sound speed profiles from the Navy's Generalized Digital Environmental Model (GDEM) for the four regions selected for this study were calculated and plotted against each of the monthly profiles to examine seasonal variability of the GDEM sound speed profiles. One specific location representing one sound speed profile was selected for each region.

The first location is a small region with a Rock Bottom type located in the mid-eastern Yellow Sea (Region 1). The sound speed profile for the annual mean at this location has a negative sound speed gradient from the surface to the bottom, thus having the characteristic of a thermocline that extends through the water column (Fig. 5). The winter months of January through March contain sound speed profiles that are relatively isothermal with a slight positive gradient. In the first month of spring, April, the sound speed gradient begins to become negative and take the form of a thermocline very similar to the annual mean by the month of May. The sound speed gradient continues to become more negative from June to the summer month of August. Then in September, the sound speed gradient becomes less negative. In the fall month of November, a mixed layer with a surface duct is generated and by December, the sound speed profile has returned to the isothermal conditions of winter.

The second location is a small region with a Gravel Bottom type located in the northeastern Yellow Sea (Region 2). The sound speed profiles for the annual mean and for each of the 12 months closely reflect those at the first location (Fig. 6). The most significant difference between the two locations is that the isothermal layer during the winter months in Region 2 falls below 1460 m/s

and the isothermal layer in Region 1 does not fall below 1465 m/s. The difference is accounted for the fact that Region 2 is located further north in the Yellow Sea.

The third location is a region with a Sand Bottom type, (the predominant bottom type for most of the western coast of the Korean peninsula) located in the southeastern Yellow Sea (Region 3). Again, the sound speed profiles for the annual mean and for each of the 12 months closely reflect those in Region 1 (Fig. 7). The fourth location is a region with a Mud Bottom type, (the predominant bottom type for most of the central and eastern Yellow Sea) located in the south-central Yellow Sea (Region 4). The sound speed profiles for the annual mean and the winter, spring, and summer months are very similar to those of Region 1 (Fig. 8). During the fall months in this region, a mixed layer is present that extends to a depth of approximately 30 meters. A surface duct is present in the mixed layer of the November and December profiles. In addition, a deep isothermal layer is present at a depth of approximately 50 meters in the October and November profiles.

B. Seasonal Variability of Signal Excess

As described earlier, the environmental effects on the performance of the AN/SQQ-32 mine hunting sonar system is being simulated by the CASS/GRAB model. This system is a variable depth high frequency sonar system, which allows the user to place the sonar at various positions in the water column to optimize the detection of either Moored or Bottom mines (Fig. 7).

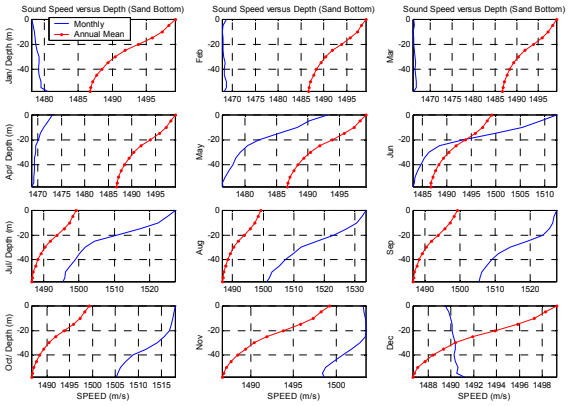

Fig. 5. Monthly and annual mean sound speed comparison for Rock Bottom for all 12 months.

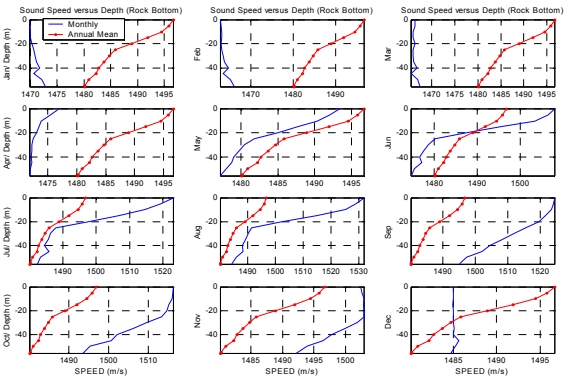

Fig. 6. Monthly and annual mean sound speed comparison for Gravel Bottom for all 12 months.

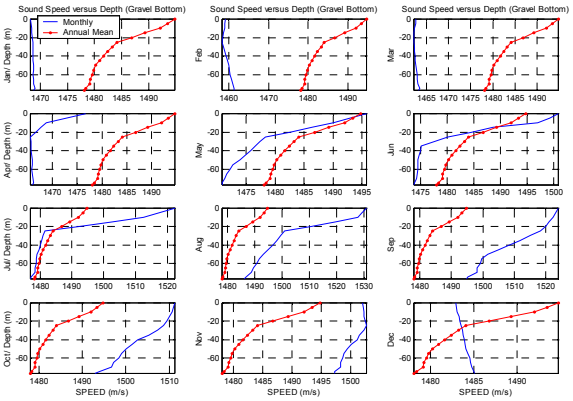

Fig. 7. Monthly and Annual Mean Sound Speed comparison for Sand Bottom for all 12 months.

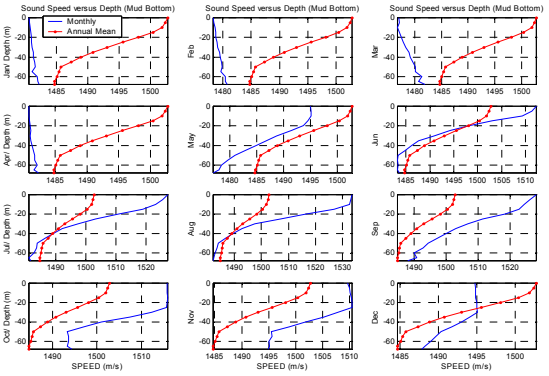

Fig. 8. Monthly and Annual Mean Sound Speed comparison for Mud Bottom for all 12 months.

In complimenting the AN/SQQ-32 mine hunting sonar system concept (Fig. 9), two source depths were chosen for feet, which places the source at the depth of a moored mine positioned for the hull depth of a large war ship. This depth also places the source within the mixed layer or surface duct to increase detection range if either is present.

The second source depth chosen was 125 feet for bottom depths greater than 135 feet, 75 feet for bottom depths between 135 feet and 85 feet, 50 feet for bottom depths

between 85 and 55 feet, and no second source depth was chosen if the bottom depth was less than 55 feet. These depths usually place the source within or below the thermocline in order to optimize detection ranges. In addition, a moderate wind speed of 5 knots and an intermediate receiver tilt angle of 8 ^{o} were used as inputs for all of the CASS/GRAB model runs in this study.

The maximum detection ranges were determined at both source depths for each month at the four different bottom type locations. In a range dependent environment such as the shallow waters of the Yellow Sea, the detection threshold is reverberation limited. Reverberation from a Rock Bottom is the highest of the four bottom types, followed by a Gravel Bottom, Sand Bottom, and Mud Bottom. Therefore, maximum detection ranges are very dependent on bottom type and bottom depths.

The maximum detection ranges for a source depth of 25 feet and a target at a depth of 25 feet were approximately 160 yards for the months of January, February, March, and December, and were approximately 120 yards for the remaining months. The reduction in the detection ranges can be attributed to the shifting of sound propagation towards the sea bottom by the thermocline present during those months, thus causing a decrease in the sound propagating in the upper water column and an increase in reverberation from the sea bottom. There were no detections for any of the months for a target located on the bottom due to the high level of reverberation and possibly the relatively large distance between the source and the ocean bottom (Figs. 10 and 11).

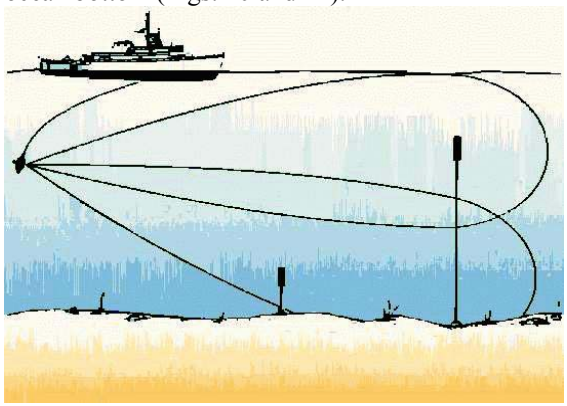

Fig. 9. AN/SQQ-32 Concept.

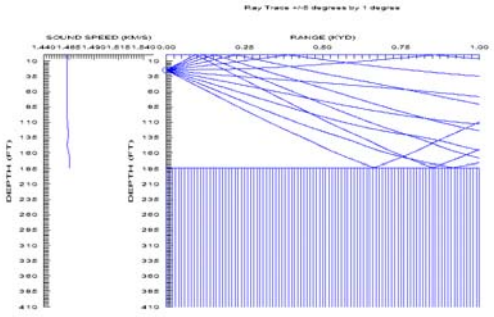

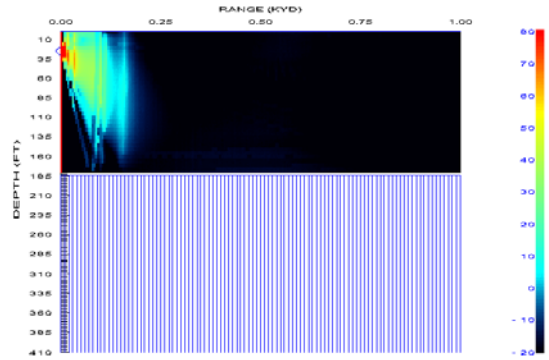

Fig. 10. Acoustic detection in February for a rock bottom at 37.5 N 123.0 E and a source depth = 25 ft. (a) ray trace and (b) signal excess.

There were no detections for any of the months for a target at a depth of 26 feet and a source depth of 125 feet. This is due to placing the source further away from a target in the upper water column and placing it closer to the sea floor thus generating a higher level of bottom reverberation. The maximum detection ranges for a target on the bottom and a source depth of 125 feet were approximately 55 yards for the months of January, February, March, April, and December, and approximately 35 yards for the remaining months. The decrease in the detection ranges from May through November is due to the source situated under the main thermocline, causing the sound propagation to be trapped between the main thermocline and the bottom, thus generating a high level of reverberation from the sea floor (Figs. 12 and 13).

The maximum detection ranges for Region 2 were also relatively short due to the high level of bottom reverberation generated by the Gravel Bottom. The maximum detection ranges for a source depth of 25 feet and a target depth of 26 feet were approximately 250 yards for the months of January, February, March, October, November, and December, approximately 150 yards for the months of April, May, and June, and approximately 225 yards for the months of August and September.

Again, these very small detection ranges can be contributed to the higher level of reverberation the receiver is exposed to by lowering it closer to the bottom ocean bottom. In this scenario, the increase in the detection ranges for the months of April through November may be attributed to the thermocline shifting sound propagation into the sea bottom and generating a bottom bounce, thus directing sound propagation towards the target in the upper water column. There were no detections for a target at the bottom for source depth of 125 feet. This may be due to the water depth at this location being deeper than in Region 1 by 20 meters, thus causing the receiver to be to far away from a bottom target to detect through the strong bottom reverberation.

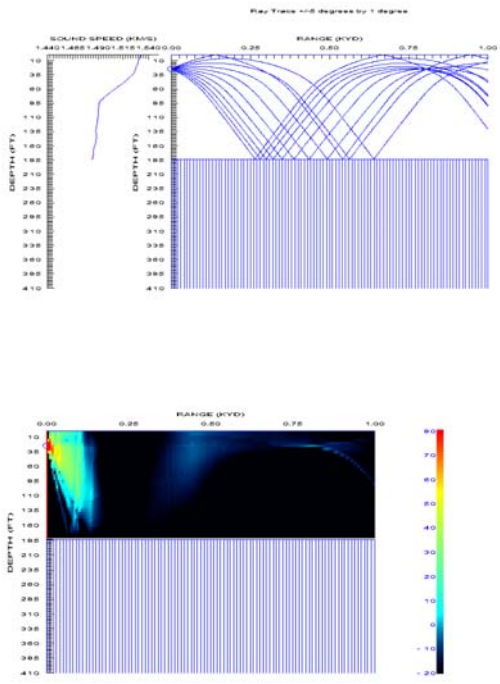

Fig. 11. Acoustic detection in August for a rock bottom at 37.5 N 123.0 E and a source depth = 25 ft. (a) ray trace and (b) signal excess.

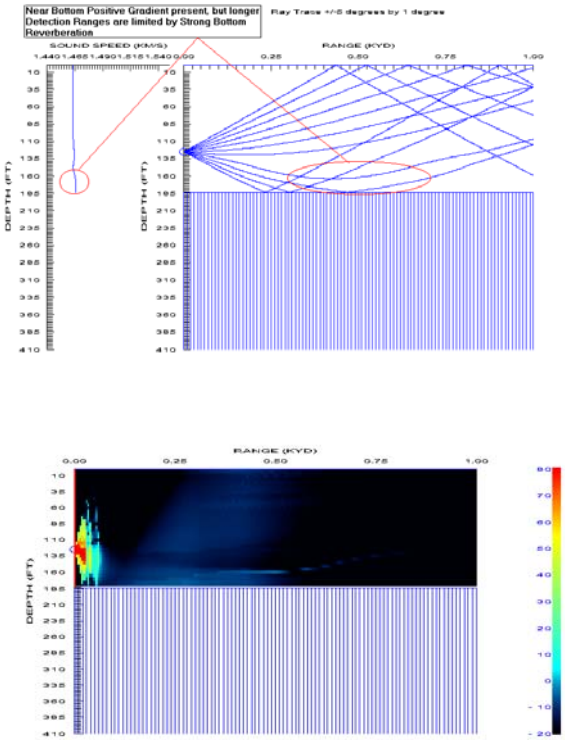

Fig. 12. Acoustic detection in February for a rock bottom at 37.5 N 123.0 E and a source depth = 125 ft. (a) ray trace and (b) signal excess.

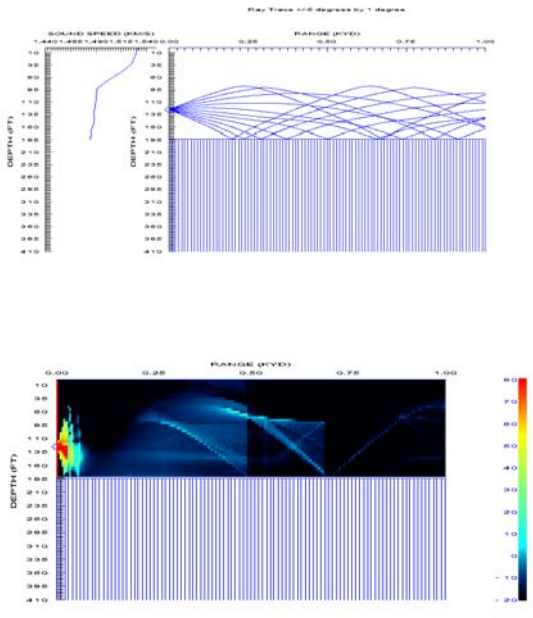

Fig. 13. Acoustic detection in August for a rock bottom at 37.5 N 123.0 E and a source depth =1 25 ft. (a) ray trace and (b) signal excess.

4. EFFECTS ON ACOUSTIC TRANSMISSION IN THE WINTER BY A STRONG COLD FRONT

The cold front chosen passed through the Yellow Sea on January 31, 2001 (Fig. 14). Mud and sand bottom regions were again chosen for this part of the study, however, at the mud region, there was a problem with near bottom positive gradients in the temperature profiles at the locations chosen earlier for the tropical depression study so profiles further north were chosen. In order to analyze the effects of the cold front in more detail, the plots of temperature and sound speed profiles for the days of January 29 through February 2, 2001 were generated for the mud region location at latitude 36.0 N longitude 123.0 E latitude (Fig. 15). The sound speed profiles show a mixed layer with a surface duct that extends to a depth of a little over 20 ft. on January 29, but shoals to a depth of 10 ft. from January 30 through February 2. This may be due to SSH data being left out of the MODAS model, since the mixed layer would not be expected to shoal with the type of winds generated by a strong cold front.

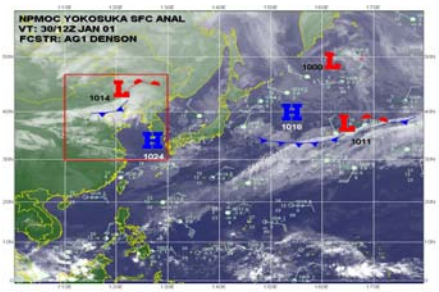

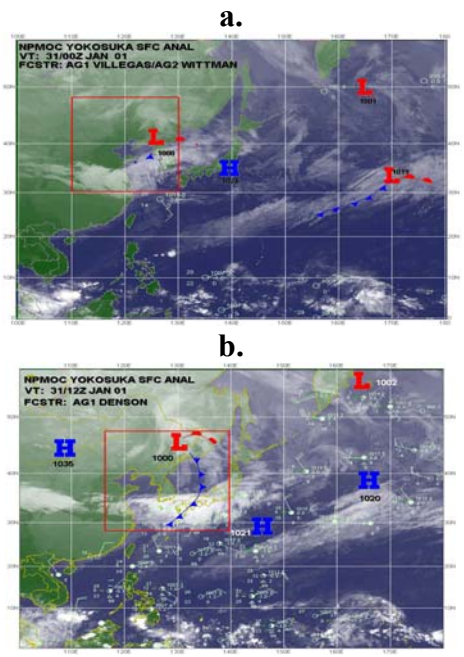

Fig. 14. Weather Maps of Cold Front moving through Yellow Sea: a. January 30, 2001/1200Z, b. Jan 31, 2001/0000Z, January 31/1200Z. (From Naval Meteorology and Oceanography Command 2000).

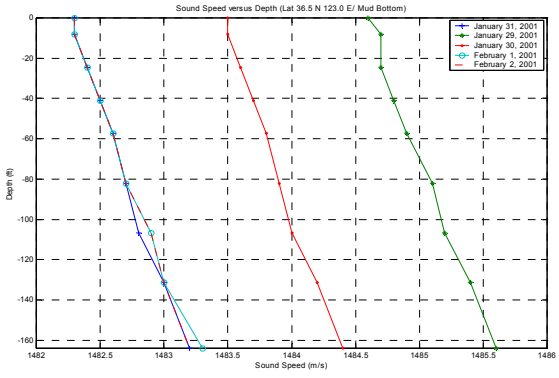

Fig. 15. Sound Speed Profiles on January 29 (green solid), January 30 (red solid), January 31 (blue solid), February 1 (green dashed), and February 2 (red dashed).

There were no significant acoustic differences produced by the CASS/GRAB model for any of the scenarios for the profiles in either region. There was, however, a significant acoustic difference observed for a source depth of 25 feet and target depth of 21 feet in the mud region for the sound speed profiles at latitude 36.0 N longitude 123.0 E, and latitude 37.0 N longitude 124.0 E. The detection ranges for January 29 for both profiles had detection ranges for a 21 feet target of over 1000 yards. The detection ranges for January 31 and February 2 were 160 yards at latitude 36.0 N longitude 123.0 E, and 260 yards at latitude 37.0 N longitude 124.0 E. The reason for the large difference in detection ranges on January 29 was that both locations had sound speed profiles that contained surface ducts, which were not present in the profiles of the other days. These sound speed profiles also contained deeper mixed layers than the sound speed profiles of January 31 and February 2.

5. ACOUSTIC UNCERTAINTY CAUSED BY HYDROGRAPHIC DATA UNCERTAINTY

A. Gaussian Type Errors in Sound Speed Profiles

The sensitivity of the CASS/GRAM model to uncertainty by hydrographical uncertainty was analyzed. The uncertainty in the hydrographic data is in the form of small or large errors that may be present in the sound speed profiles possibly due to the accuracy of the instruments used to obtain the data, the expertise of the person obtaining the data, and in the case of MODAS, the accuracy of the algorithms in the model.

To simulate hydrographic data uncertainty, a MATLAB code was used to randomly enter a various range Gaussian-type error into the MODAS sound speed profiles. The MATLAB code was written to allow the user to enter the desired size of the error to be entered into the sound speed profiles to be studied. Three sizes of errors, 1, 5, and 10 meters per second, were entered into the sound speed profiles and then inputted into the CASS/GRAB model. The regions selected for this study were mud and sand. February and August were chosen to capture the effects of the error on the two main sound speed profile structures of the Yellow Sea.

B. Corresponding Errors in Signal Excess

The CASS/GRAB model was run using the MODAS profiles with the three level of errors. The runs were performed for a source of 25 feet and 125 feet. The maximum detection ranges derived from the signal excess (SE) calculations of the model were compared to those of the MODAS sound speed profile runs without error by taking the absolute deference of MODAS profiles without error and the corresponding MODAS profiles with error to determine if a significant acoustic difference existed. The results were that a significant acoustic difference was observed in all of the scenarios for both bottom types, with the exception of the scenarios of a 25 feet source depth and bottom target, and a 125 feet source depth and a 26 feet target depth in the mud region during the summer. In order to further illustrate the sensitivity of the CASS/GRAB model to small sound speed errors near the source, a random error with amplitude of 1 m/s was added into the MODAS sound speed profile at the source depths of 25 ft (Fig. 16) and 125 ft (Fig. 17). A shadow zone was formed in front of the source that significantly decreased the detection ranges at that depth, and when the error (1m/s) error was added at both source depths, a strong sound channel formed that dramatically increased detection ranges at that depth.

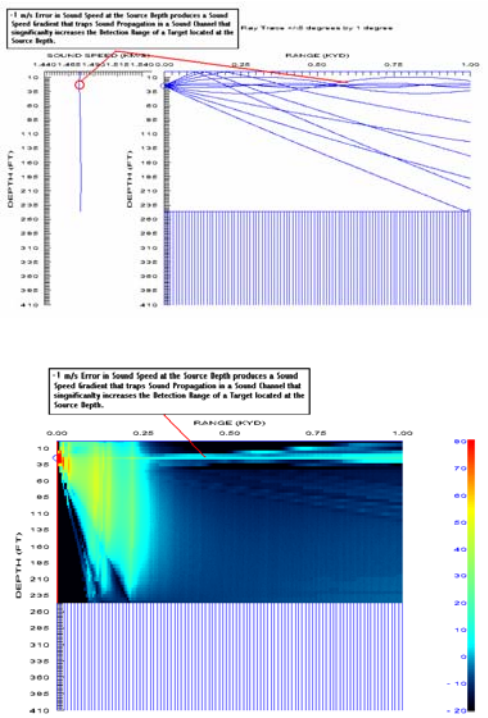

Fig. 16. Effect of error (-1 m/s) added to the sound speed profile at the source depth (25 ft) for February 15, 2000, 36.4 N 124.4 E, mud bottom: (a) ray trace, (b) signal excess (maximum detection range at the source depth >1000 yd, Δ max detection range at the source depth >740 yd).

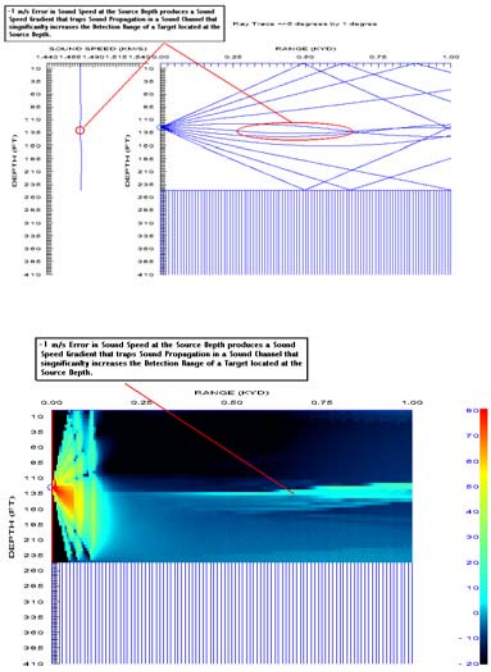

Fig. 17. Effect of error (-1 m/s) added to the sound speed profile at the source depth (125 ft) for February 15, 2000, 36.4 N 124.4 E, mud bottom: (a) ray trace, (b) signal excess (maximum detection range at the source depth >1000 yd, Δ max detection range at the source depth >855 yd).

Thus, the CASS/GRAB sensitivity to error in sound speed profiles was very dependent on the location of that error in relation to the source. In addition, CASS/GRAB is more sensitive to errors in the isothermal structure of the sound speed profiles characteristic of the winter months. This sensitivity was due to the introduction of either a positive or negative sound speed gradient by the error to a linear sound speed structure.

6. CONCLUSIONS

In this study, the seasonal variation in acoustic transmission in the Yellow Sea for all regions was mainly due to the isothermal structure in the winter and a multi-layer thermal structure in the summer. The acoustic transmission in the winter is shorter due to the effect of the isothermal structure of the sound speed profile, thus detection ranges are shorter. The acoustic transmission in the summer is significantly longer due to the down bending effects of the multi-layer structure of the sound speed profiles, which produce convergence zone and caustics.

Since there is a significant effect to acoustic transmission by environmental factors as demonstrated by the seasonal variability and the hydrographical data set comparisons, the conclusion is that there is a need for a predictive modeling capability such as MODAS to address the MIW needs in the Yellow Sea region. Although MODAS is the best model available at this time to meet the MIW needs, the model demonstrated some limitations in the Yellow Sea. In many cases the MODAS profile did a good job in producing profiles that reflected changes in the climate, but for the reasons stated earlier it sometimes under predicted the effects of the changes in the climate. There were also problems with inaccurate profiles that related to the limitations of the MODAS climatology.

The most significant problem with the climatology that generated an acoustic difference was detected in the winter months in the southern region of the Yellow Sea. Many of the MODAS temperature and sound speed profiles had near bottom positive gradients below an isothermal layer, which was not observed in NIDAS for any of the MOODS profiles in the Yellow Sea regions studied. This downward positive gradient in MODAS caused an under prediction in detection ranges for Bottom mines due to the up bending of sound propagation near the sea bottom. In the case of a near surface volume mine (moored mine), this up bending produced less bottom reverberation, thus causing an over prediction of the detection ranges of these mines. Since this near bottom downward positive gradient was present in both the 1999 and 2000 MODAS profiles used, the cause may be due to the sparseness of observational data along the shelf located between the southern Yellow Sea and the northern East China Sea for use in developing the MODAS climatology. Since the MODAS climatology data sets were not available for analysis during this study, this conclusion is speculation.

Another problem that was a major source of significant acoustic difference was observed in the summer months. Although MODAS profiles did capture surface ducts in the mixed layer, they were much weaker than expected, and much weaker than those observed in most of the MOODS profiles. The weaker surface duct caused an under prediction of moored mines when the source was at hull depth. In many cases, MODAS tended to weaken the thermocline gradient found in many of the MOODS profiles during the summer months. This weakening of the thermocline gradient produces less down bending of sound propagation. This in turn produces less focusing of sound propagation, which translates into the under prediction of detection ranges.

The CASS/GRAB sensitivity to error in sound speed profiles was very dependent on the location of that error in relation to the source. In addition, CASS/GRAB is more sensitive to errors in the isothermal structure of the sound speed profiles characteristic of the winter months. This sensitivity was due to the introduction of either a positive or negative sound speed gradient by the error to a linear sound speed structure.

NAVOCEANO has been working with numerical ocean models to fix the problems with MODAS altimeter SSH data input in shallow water region. They hope to implement this SSH correction into the MODAS within the next couple of years. In addition, NAVOCEANO is developing a new MODAS climatology that will correct some of the problems in climatology that were mentioned earlier. These new improvements into the MODAS model will show a significant improvement to the models performance in shallow waters regions thus increasing the utility of the model for MIW applications in shallow water.

Suggested future work in studying the environmental effects on mine hunting in the Yellow Sea using the CASS/GRAB model are as follows: 1. Comparing the MODAS climatological profiles (Static MODAS) with the corresponding synthetic MODAS profiles (Dynamic MODAS), 2. Comparing recent XBTs with corresponding synthetic MODAS profiles, and 3. Performing various studies with Bathymetry data entered into the CASS/GRAB model.

ACKNOWLEDGMENT

We wish to acknowledge the following individuals who were responsible for making this research possible: Chenwu Fan at the Naval Postgraduate School; and Dan Fox at the Naval Research Laboratory.

This work was supported by the Naval Oceanographic Office, and the Naval Postgraduate School.

REFERENCES

Aidala, F.E., Keenan, R.E., and Weinberg, H., Modeling high frequency system performing in shallow-water range-dependent environments with the comprehensive acoustic simulation system (CASS). NUWC Division Newport Technical Digest, 54-61, 1998.

Chu, P. C., Wells, S. K., Haeger, S. D., Szczechowski, C., and Carron, M. J., Temporal and Spatial Scales of the Yellow Sea Thermal Variability. Journal of Geophysical Research, 102, C3, 5657-5658, 1997a.

Chu, P. C., Fralick, C. R., Haeger, S. D., and Carron, M. J, A Parametric Model for the Yellow Sea Thermal Variability. Journal of Geophysical Research, 102, C5, 10499-10507, 1997b.

Chu, P. C., Tseng, H., Chang, C. P., and Chen, J. M., South China Sea Warm Pool Detected in Spring from the Navy's Master Oceanographic Observational Data Set (MOODS). Journal of Geophysical Research, 102, C7, 15761-15762, 1997c.

Fox, D. N., Teague, W. J., Barron, C.N., Carnes, M.R., and Lee, C.M., The Modular Ocean Data Assimilation System (MODAS). In preparation for: Journal of Atmospheric Oceanic Technology, pp. 4-11, 2000.

Jensen, F. B., Kuperman, W. A., Porter, M. B., and Schmidt, H., Computational Ocean Acoustics, Springer-Verlag, 2000.

Keenan, R., Weinberg, H., E., and Aidala, F. E., Software Requirements Specifications for the Gaussian Ray Bundle (GRAB) Eigenray Propagation Model. OAML-SRS-74, Systems Integration Division Stennis Space Center, MS, 1999.

Keenan, R. E., An Introduction to GRAB Eigenrays and CASS Reverberation and Signal Excess. Science Applications International Corporation, MA, 2000.

Medwin, H., and Clay, C. S., Fundamentals of Acoustical Oceanography, Academic Press, 1998.

Mississippi State Center of Air Sea Technology, User's Manual for the Naval Interactive Data Analysis System (NIDAS) Version 3.1. Technical Note 4-97, Stennis Space Center, MS, 1997.

Naval Oceanographic Office Systems Integration Division, Software Design Document for the Gaussian Ray Bundle (GRAB) Eigenray Propagation Model. OAML-SDD-74. Stennis Space Center, MS, 1999.

Naval Oceanographic Office Systems Integration Division, Data Base Description for the Generalized Digital Environmental Model (GDEM-V) Version 2.5. OAML-DBD-72C, Stennis Space Center, MS, 2000.

Naval Research Laboratory Code 7320, User's Manual for the Modular Ocean Data Assimilation System (MODAS) Version 2.1. PSI Technical Report S-285. Stennis Space Center, MS, 1999.

Naval Research Laboratory Code 7323, Confidence Level Assessment of MODAS Appendix 1: Upgraded Altimetry Processing. Stennis Space Center, MS, 2000.

Ninno, H., and Emery, K. O., Sediments of Shallow Portions of the East China Sea and South China Sea. Geology Society of America BULL., 72, pp. 731-762, 1961.

Shepard, F. P., Submarine Geology, pp. 246-250, Harper & Row, 1973.

Teague, W. J., Carron, M. J., and Hogan, P. J., A Comparison between the Generalized Digital Environmental Model and Levitus Climatologies. Journal of Geophysical Research, 95, C5, 7167-7183, 1990.

Peter C. Chu (PhD, 85') is a professor of oceanography, joint warfare analysis, and modeling and virtue environment simulation (MOVES) at the Naval Postgraduate School, Monterey, CA 93943, USA.

Carlos J. Cintron (MA, 01) is a Navy Lieutenant who obtained MA degree in Physical Oceanography at the Naval Postgraduate School in March 2001.

Steven D. Haeger (MA, 78') is the director of the ocean modeling department, Naval Oceanographic Office, Stennis Space Center, MS 39529; and an adjunct professor at the Naval Postgraduate School.

Ruth E. Keenan has 23 years experience in underwater acoustic propagation modeling and has managed SAIC office on Cape Cod for 20 years.